Lifetimes of odd-spin yrast states in ^{182}Hg

M. Scheck,[1] T. Grahn,[1] A. Petts,[1] P. A. Butler,[1] A. Dewald,[2] L. P. Gaffney,[1] M. B. Gómez Hornillos,[3,*] A. Görgen,[4] P. T. Greenlees,[5] K. Helariutta,[6] J. Jolie,[2] P. Jones,[5] R. Julin,[5] S. Juutinen,[5] S. Ketelhut,[5] T. Kröll,[7,†] R. Krücken,[7] M. Leino,[5] J. Ljungvall,[4] P. Maierbeck,[7] B. Melon,[2] M. Nyman,[5] R. D. Page,[1] J. Pakarinen,[1,‡] E. S. Paul,[1] Th. Pissulla,[2] P. Rahkila,[5] J. Sarén,[5] C. Scholey,[5] A. Semchenkov,[8,§] J. Sorri,[5] J. Uusitalo,[5] R. Wadsworth,[9] and M. Zielińska[4,10]

[1]*Oliver Lodge Laboratory, University of Liverpool, Liverpool L69 7ZE, United Kingdom*
[2]*Institut für Kernphysik, Universität zu Köln, Zülpicher Str. 77, D-50937 Köln, Germany*
[3]*STFC, Daresbury Laboratory, Warrington WA4 4AD, United Kingdom*
[4]*CEA-SACLAY, DSM/DAPNIA/SPhN, F-91191 Gif-Sur-Yvette Cedex, France*
[5]*Department of Physics, University of Jyväskylä, P.O. Box 35, FI-40014 Jyväskylä, Finland*
[6]*Laboratory of Radiochemistry, Department of Chemistry, P.O. Box 55, FI-00014 Helsinki, Finland*
[7]*Physik-Department E12, TU München, D-85748 Garching, Germany*
[8]*GSI, D-64220, Darmstadt, Germany*
[9]*Department of Physics, University of York, Heslington, York YO10 5DD, United Kingdom*
[10]*Heavy Ion Laboratory, University of Warsaw, PL-02097 Warsaw, Poland*

(Received 4 November 2009; published 22 January 2010)

Lifetimes of excited states in ^{182}Hg were extracted from recoil-gated γ-ray spectra and recoil-gated $\gamma\gamma$-coincidence matrices using the recoil distance Doppler-shift method. States were populated using the ^{96}Mo(^{88}Sr,2n)^{182}Hg fusion-evaporation reaction. Measured lifetimes allowed transition probabilities, transition quadrupole moments, quadrupole deformation parameters, and transition dipole moments to be deduced for the band formed by the odd-spin yrast states. The experimental results confirm the low degree of octupole collectivity in this mass region.

DOI: 10.1103/PhysRevC.81.014310 PACS number(s): 21.10.Tg, 21.10.Ky, 23.20.Lv, 27.70.+q

I. INTRODUCTION

The mass region of neutron-deficient Hg and Pb isotopes near the neutron midshell ($N = 104$) is well known for the phenomenon of shape coexistence [1,2]. Due to this very interesting feature the nuclei in this part of the nuclear landscape are subject to strong experimental and theoretical efforts (see Ref. [3] and references therein). In the light Hg isotopes, the ground states and low-spin states of the even-spin yrast band are associated with a slightly deformed oblate shape, while high-spin yrast states belong to a more deformed prolate band. In a shell-model approach, the oblate structure is built on two proton hole $\pi(2h)$ and neutron configurations. The prolate band has a proton intruder configuration, where two protons are excited across the $Z = 82$ shell closure, forming a two-particle four-hole configuration $\pi(2p4h)$ [4] coupled with the respective neutron components. In mean-field calculations [5–7], the potential energy surface (PES) shows two distinct minima of which the global one, situated at $\beta_2 \approx -0.15$, represents the oblate deformation and a local minimum found at $\beta_2 \approx 0.27$ is associated with the coexisting prolate shape. The theoretically predicted values of the deformation parameters $|\beta_2|$ for the two bands were confirmed experimentally from lifetime measurements, which were performed using the recoil distance Doppler-shift method (RDDS) for low-spin states in ^{180,182}Hg [8], ^{184}Hg [9], ^{186}Hg [10], and the Doppler-shift attenuation method (DSAM) for high-spin states in ^{186}Hg [11].

The level energy systematics of the even-spin yrast states [shown in Fig. 1(b)] exhibit a parabolic behavior of the intruder configuration between the mass numbers 176 and 188. From the level sequences it is obvious that states of a given angular momentum belonging to either of the two even-parity bands mix when they lie close in energy. Several attempts were made to determine the degree of mixing for the low-spin states in the light Hg isotopes. The different approaches use the $\rho(E0)^2$ strength [13] of $E0$ transitions connecting states of the same angular momentum of both bands [14], the observed hindrance factors for the α decay from the respective mother nucleus [15], or the deviations of the observed excitation energies of the first 2^+ states from the general systematics in the mass region of interest [16]. Recently, a further study deduced the degree of mixing from the lifetimes in ^{180,182}Hg [8]. However, the different methods result in considerably deviating values.

In this mass region, bands with a proposed negative parity were also observed (e.g., see Refs. [17,18] and references therein). From a microscopic point of view negative parity excitations benefit from the Fermi level within the neutron $i_{13/2}$ unique-parity subshell. For the nuclei under investigation, the quadrupole part of the residual proton-neutron interaction weakens the $Z = 82$ shell gap. This allows proton orbitals from above the $Z = 82$ shell closure to approach the Fermi level and opens the possibility for further negative-parity two-quasiparticle excitations. On the other hand, the general systematics of $B(E3, 0_1^+ \rightarrow 3_1^-)$ strengths (e.g., Fig. 24 in

*Present address: Department of Physics and Nuclear Engineering, Universitat Politécnica de Catalunya, Barcelona, Spain.
†Present address: Institut für Kernphysik, TU Darmstadt, D-64289 Darmstadt, Germany.
‡Present address: ISOLDE group, CERN, Switzerland.
§Present address: University of Oslo, Oslo, Norway.

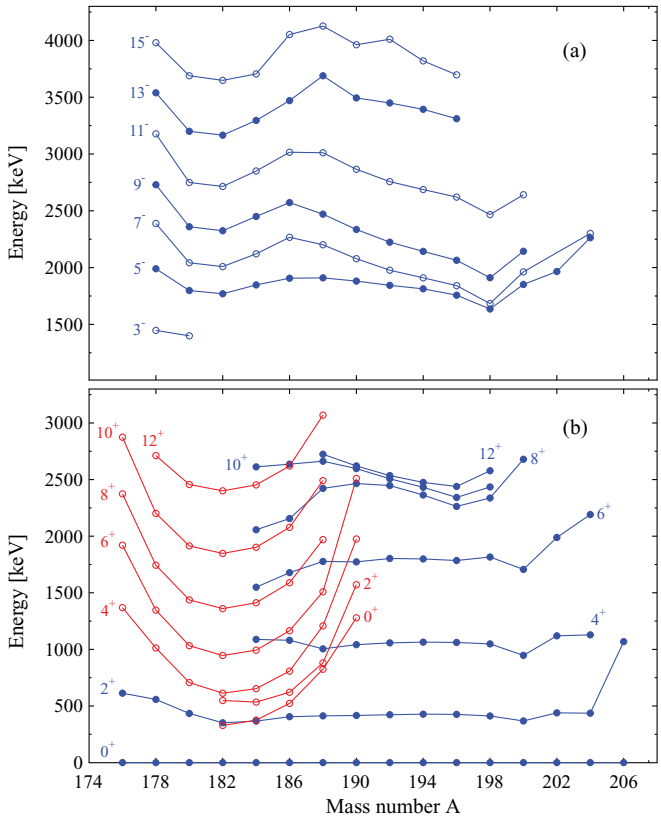

FIG. 1. (Color online) (a) Energy systematics of odd-spin yrast states in even-mass Hg isotopes. Please note the 1 MeV offset of the *y* axis. (b) Systematics of low-lying positive parity states in even-mass Hg isotopes. The level energies of states with an assumed oblate deformation are shown with full (blue) symbols. Level energies of states with an assumed prolate shape are shown with open (red) symbols. The data are taken from the NNDC data base [12].

Ref. [19] or Figs. 1 and 2 in Ref. [20]) point toward a rather low octupole collectivity in this mass region.

For ^{178}Hg [21] and ^{180}Hg [17] candidates for $J^\pi = 3^-$ octupole excitations are proposed. Previous studies of

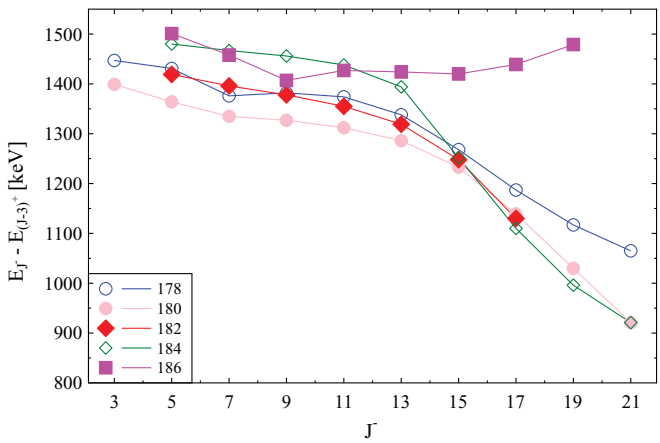

FIG. 2. (Color online) Energy differences for states of the odd-spin band and the even-spin yrast states with a difference of three units of angular momentum.

^{182}Hg [22] and ^{184}Hg [23] did not propose candidates for an octupole excitation. A candidate in ^{186}Hg was found at 1228 keV [24], but a second study [25] assigned a spin and parity of $J^\pi = 4^+$ to this state. From the level-energy systematics band 8 in Fig. 1 of Ref. [25] exhibits a similar behavior to the odd-spin bands under investigation. However, in ^{186}Hg no decay to an octupole candidate was observed.

In ^{178,180}Hg the respective 3^- candidates are populated by decays stemming from 5^- states, which is the bandhead of an odd-spin band. Due to the decay behavior a firm assignment of negative parity was given to these bands [17]. Considering the striking similarity of the odd-spin bands of ^{180}Hg and ^{182}Hg, up to spin $J^\pi = 15^{(-)}$ with almost identical transition energies (see Fig. 2 in Ref. [17] and Fig. 3 in Ref. [22]), a negative parity of the odd-spin band in ^{182}Hg is probable. As shown in Fig. 1(a), the excitation energies of the observed odd-spin bands of even-even $^{178-186}$Hg show a similar pattern to the even-spin yrast states. The excitation energy of a state of a given angular momentum J^π exhibits a slightly parabolic behavior for isotopes near the neutron midshell at $N = 104$. Figure 2 shows the difference of the excitation energies of the states of a given angular momentum $J^{(-)}$ belonging to the odd-spin band and the state with $(J-3)^+$ of the even-spin yrast band. Up to spin $J^\pi = 13^{(-)}$, constant energy differences at approximately the excitation energy of the respective octupole candidate are observed. This supports the suggestion given in Ref. [17] that the bands are based on an octupole excitation aligned with the even-spin yrast band. Above spin-13 the energy differences decrease. The alignment plots (e.g., Fig. 6 in Ref. [17]) show an alignment of about three units for the low-spin. The band is then crossed by a shape-driving two-quasiparticle excitation resulting in an additional alignment gain of five units. However, the corresponding odd-spin band in ^{186}Hg does not follow the systematic behavior of the bands observed in the other isotopes as the energy difference $E_{J^-} - E_{(J-3)^+}$ remains constant.

So far, apart from the $J^\pi = 9^-$ state in ^{180}Hg [8], no lifetimes for low-spin members of these particular bands in even-even $^{178-186}$Hg are known. The observed lifetime in ^{180}Hg results in a similar quadrupole deformation for the odd-spin state ($|\beta_2^t| = 0.27$) as observed for the even-spin yrast states with $J \geqslant 4$. Measured lifetimes together with observed branching ratios will allow the extraction of transition quadrupole moments $|Q_t|$ and the degree of quadrupole deformation $|\beta_2^{(t)}|$ from the intraband transition matrix elements $\langle\Psi(J^-)|E2|\Psi(J+2^-)\rangle$. Furthermore, the transition dipole moments $|D_t|$ can be determined from the $E1$ interband transitions matrix elements $\langle\Psi(J^+)|E1|\Psi(J\pm1^-)\rangle$.

In Sec. II a short overview of the experimental setup and technique is given, the experimental results are presented in Sec. III and the experimental findings will be discussed in Sec. IV.

II. EXPERIMENTAL SETUP AND TECHNIQUE

The data presented in this work were obtained as a by-product of the work published in Ref. [8]. Therefore, only a

short introduction of the setup and experimental technique will be given.

The experiment was conducted at the Accelerator Laboratory of the University of Jyväskylä. Excited states in ^{182}Hg were populated by bombarding a 0.8 mg/cm^2 thick ^{96}Mo target with a beam of 310 MeV ^{88}Sr^{16+} ions. The average beam current was 2 pn$A$. The reaction kinematics resulted in a recoil velocity of $v/c = 4.4\%$ for the ^{182}Hg residues.

Prompt γ rays were detected using the JUROGAM array, consisting of 43 Compton-suppressed high-purity Ge detectors placed into several rings. The rings are distinguished by their angle to the direction given by the incident beam. At the target position the Köln plunger device was installed for lifetime measurements applying the RDDS technique. To be able to clean the prompt γ-ray spectra from residues of other reaction channels and fission background, the standard stopper foil of the plunger was replaced with 1 mg/cm^2 Mg degrader foil to allow the ^{182}Hg nuclei to enter the gas-filled Recoil Ion Transport Unit (RITU) separator [26]. At the focal plane of RITU, the GREAT spectrometer [27] was utilized for the recoil-gated tagging technique. GREAT consists of a multiwire proportional counter (MWPC) to record the energy loss and timing information of the recoiling nuclei and a pair of double-sided silicon strip detectors (DSSDs) in which the recoils are implanted. Energy loss and timing information of the MWPC and DSSDs are used to select recoil evaporation residues. The data were collected with the total data readout triggerless data acquisition system [28]. The software package GRAIN [29] was utilized to produce the recoil-tagged spectra and $\gamma\gamma$-coincidence matrices. Due to the comparatively long half-life of ^{182}Hg ($T_{1/2} = 10.83(6)$ s [30]) and the low α-decay branching ratio a further application of decay tagging with the α-decay energies measured in the DSSDs was not possible.

For the lifetime analysis, the JUROGAM rings 2 (134°, 10 detectors) and 1 (158°, 5 detectors) were used. The lifetimes were deduced from the two sets of singles γ-ray spectra taken at 15 different target-to-degrader distances and from the corresponding $\gamma\gamma$-coincidence matrices. Examples of singles spectra are shown in Fig. 3 and examples of axis-projected spectra from the $\gamma\gamma$-coincidence analysis are shown in Fig. 4. To exclude perturbing effects due to side feeding, the projected spectra for the $\gamma\gamma$-coincidence measurement were gated on the direct feeding transition. Furthermore, to raise the level of statistics in the spectra it was necessary to include in the gates both peaks corresponding to the degraded and fully-shifted component of the γ-ray transition. For both analysis methods the peak areas of the degraded [$I_d(d)$] and the fully-shifted component [$I_f(d)$] of a given transition were normalized to the sum of both [$I_d(d) + I_f(d)$] and the decay curve as a function of the distance between the reaction target and the degrader foil are plotted. The final lifetime analysis was performed applying the differential decay curve method (DDCM) [31]. A sample plot obtained in the matrix analysis is shown in Fig. 5.

III. EXPERIMENTAL RESULTS

The level scheme as published in Ref. [22] was checked using the 90° matrix, which is a combination of the

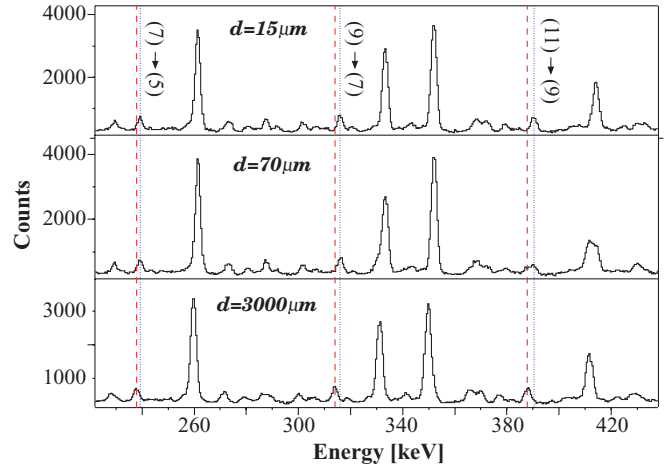

FIG. 3. (Color online) Singles recoil-gated spectra recorded under three different target-to-degrader distances using ring 2 of the JUROGAM array. The lines are to guide the eyes for the distance-dependent shift of peaks stemming from transitions of interest for this work.

$\gamma\gamma$ matrices obtained using the data collected in the JUROGAM rings 4 (94°) and 5 (86°). A total of 5.1×10^5 $\gamma\gamma$ coincidences were recorded. The relative intensities $I_{\rm rel}$ were determined with the projection of this symmetric matrix, as shown in Fig. 6.

The relative intensities, normalized to the 351.7-keV transition, are given in two different tables. Table I contains the transitions that are shown in the level scheme of ^{182}Hg in Fig. 3 of Ref. [22]. Table II includes transitions that were found in the spectra, but are of unknown origin. Possible sources are, of course, ^{182}Hg itself, especially prompt decays from structures built on a high-K isomer as observed for ^{184,186}Hg [23,25], or other transitions that so far have not been placed in the level scheme. One should consider that the

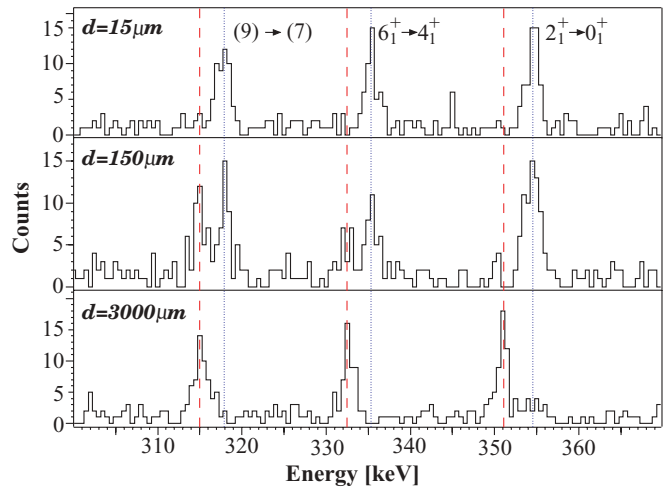

FIG. 4. (Color online) Axis-projected recoil-gated $\gamma\gamma$ spectra recorded under three different target-to-degrader distances and created by gating on the 390 keV transition in the corresponding matrices. The matrices were recorded with the detectors of ring 1 of the JUROGAM array.

TABLE I. Relative intensities of the γ-ray transitions observed in the projection on the y axis of the full 90° matrix. Only transitions are included that are given in Fig. 3 of Ref. [22]. The intensities were normalized to the 351.7-keV transition.

E_γ [keV]	ΔE_γ [keV]	I_{rel}	ΔI_{rel}
183.9	0.8	4.2	0.6
239.4	0.4	11.7	1.2
261.5	0.3	84.5	5.9
301.8	0.4	7.5	0.8
315.9	0.4	14.4	1.3
333.1	0.3	71.8	5.0
351.7	0.3	100	–
372.2	0.5	9.7	1.8
379.1	0.4	7.2	0.9
389.9	0.4	16.4	1.5
413.7	0.3	54.1	4.3
424.4	0.5	6.3	0.9
447.2[a]	0.5	9.2	1.3
452.1	0.4	15.3	1.5
462.0	0.5	8.1	1.1
466.6	0.6	6.6	1.1
471.9	0.4	12.7	1.5
481.5	0.6	5.6	1.5
487.0	0.4	33.6	3.1
493.4	0.5	9.3	1.1
512.1[a]	2.9	11.7	4.8
516.6[a]	1.0	9.0	2.8
527.2	4.4	1.6	1.6
548.3	0.5	16.1	2.4
552.5	0.5	27.5	3.0
557.1	0.9	5.3	1.4
567.8	0.9	2.9	0.7
576.5[a]	0.6	6.7	1.0
586.3[a]	0.4	15.0	1.6
610.7	0.6	16.5	2.8
627.5	0.6	8	1.2
661.4	0.5	9.1	1.2
682.2	1.0	2.2	0.6
706.8	0.9	2.6	0.6
748.2	0.5	9.8	1.3
771.8	0.8	12.8	1.8
816.7	0.6	6.3	0.9
850.7	0.8	4.6	0.9
867.5	1.0	2.5	0.6
963.0	0.7	5.3	0.8
1060.9	0.7	3.2	0.6
1156.7	1.0	2.4	0.7

[a]Peak contains contaminations from other transitions.

band built on the oblate-deformed ground state was observed in ^{182}Hg. Furthermore, transitions of contaminating other reaction products are possible. Transitions that were firmly identified as belonging to other reaction products, such as ^{183}Hg ($1n$ channel) [32,33], ^{184}Hg (direct reaction product) [23], ^{183}Au ($1p$ channel) [34–36], and ^{181}Au ($p2n$ channel) [34,37] were neglected in the tables.

Due to the low number of $\gamma\gamma$-coincidence events and the resulting lack of statistics only minor improvements for the level scheme as known in the literature [22] could be made. The previous tentative placement of the 576.5-keV γ ray as transition feeding the first 2_1^+ state was shown to be wrong. Instead of placing this transition as decaying to the first 2_1^+ state at 351.7 keV, we propose a placement as a decay to the second 2_2^+ state at 548.3 keV. Indeed the background-corrected coincidence spectrum (see Fig. 7) confirms such a placement.

TABLE II. Intensities of γ-ray transitions observed in the projection on the y axis of the full 90° matrix, but not previously observed in ^{182}Hg or firmly identified as belonging to another reaction product. The intensities were normalized to the 351.7-keV transition given in Table I. For a more detailed discussion see text.

E_γ [keV]	ΔE_γ [keV]	I_{rel}	ΔI_{rel}
105.2	1.9	2.6	0.6
127.0	1.8	3.3	0.6
130.4	1.6	2.3	0.5
133.8	1.4	2.5	0.5
138.2	1.2	1.7	0.4
149.7	1.2	2.0	0.6
152.4	1.3	1.6	0.6
169.7	0.9	2.4	0.5
174.4	0.9	2.4	0.5
178.7	0.9	2.8	0.5
187.2	0.9	3.2	0.5
199.5	1.0	1.9	0.4
209.9	0.5	3.4	0.6
232.4	0.6	2.0	0.5
243.1	0.6	2.0	0.4
247.8	0.5	2.3	0.5
251.9	0.5	2.9	0.5
257.2	0.5	5.4	0.8
280.8	0.4	5.5	0.7
292.0	0.5	3.8	0.6
306.4	0.5	4.0	0.6
320.9	0.5	3.1	0.5
338.3	0.5	3.0	0.5
369.5	1.6	3.7	2.6
383.3	0.6	2.5	0.5
439.0	0.7	2.8	0.6
443.7	0.7	4.9	1.0
500.1	0.6	5.6	0.9
510.4	3.5	8.0	6.1
523.0	1.9	3.4	1.7
593.3	0.7	5.3	0.9
616.2	1.0	3.2	0.9
634.7	1.6	2.4	0.8
640.7	1.4	2.2	0.8
753.9	1.0	2.7	0.7
765.4	1.4	1.6	0.7
837.0	0.8	3.1	0.7
844.8	0.7	6.0	1.0
917.7	1.0	3.1	0.7
1011.3	1.5	2.2	0.6
1018.0	0.8	2.6	0.6
1200.6	1.6	2.1	0.6
1210.0	3.3	1.5	1.1
1222.8	2.3	1.7	0.8
1241.7	2.2	1.5	0.7

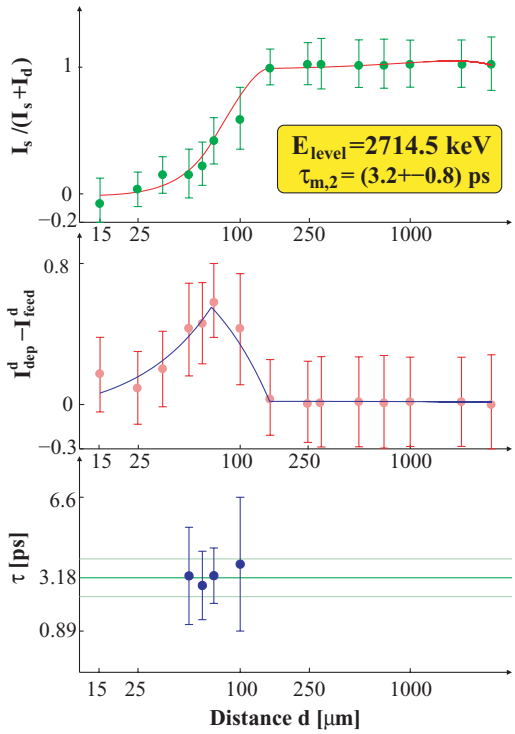

FIG. 5. (Color online) Example of a lifetime determination using the $\gamma\gamma$-coincidence matrices of the JUROGAM ring 2 detectors for the $J = 11^{(-)}$ level at 2714.5 keV. The upper panel shows the fit of the normalized shifted component of the depopulating transition ($E_\gamma = 390.0$ keV). In the middle panel the fit to the difference between the degraded components of feeding ($E_\gamma = 451.9$ keV) and depopulating transitions is shown. The final lifetime results for each of the used gradients at four target-to-degrader distances d is given in the bottom panel.

This placement results in a new level at 1124.8 keV. A possible decay of this level to the first 2^+_1 state, as can be expected due to the obvious mixing of the two first excited 2^+_i levels ($i = 1, 2$), will have a transition energy of $E_\gamma = 773.1$ keV.

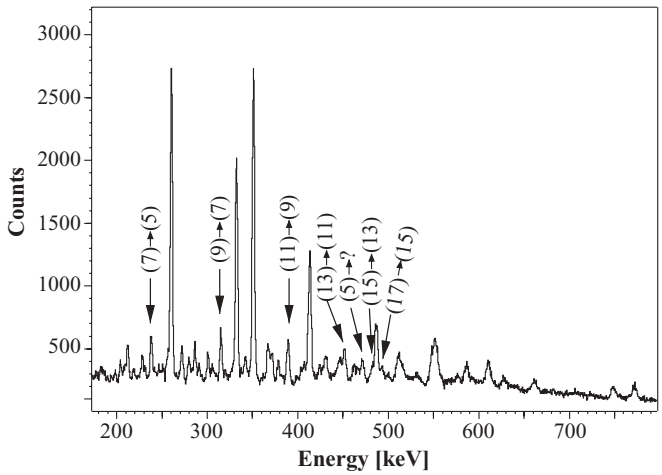

FIG. 6. Full projection of the symmetric 90° matrix on the y axis. Peaks associated with intraband transitions of the odd-spin band in ^{182}Hg are labeled.

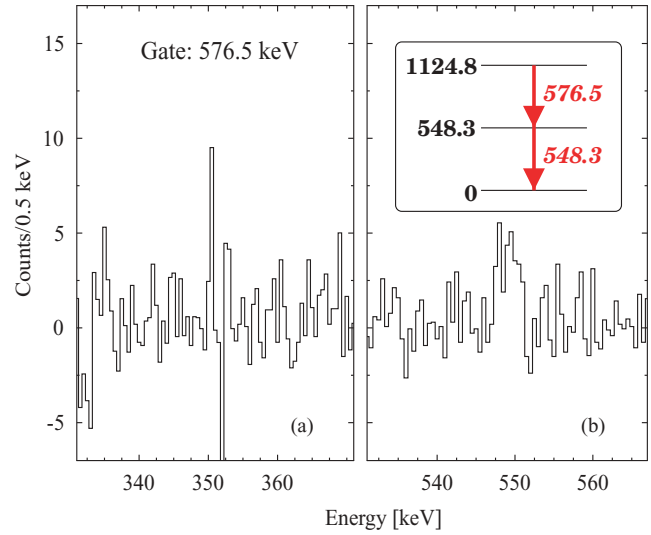

FIG. 7. (Color online) Parts of the spectrum created by gating on the 576.5-keV transition of the 90° matrix. Clearly (a) the 351.7-keV transition depopulating the first 2^+_1 state is suppressed, while (b) the 548.3-keV transition depopulating the second 2^+_2 state is still present. The new placement of the 576.5-keV γ ray in the level scheme is shown in the insert.

At the current level of statistics it is not possible to distinguish this possible transition from the strong 771.8 keV transition populating the 4^+_1 yrast state. A reverse gate on the $2^+_1 \rightarrow 0^+_{gs}$ transition cannot clarify the situation. The final level of the dominating, covering transition is another yrast state. Thus this transition also appears in the gated spectra. The proposed state at 1124.8 keV is, from the energy systematics of the even-even Hg isotopes [see Fig. 1(b)], a good candidate for the 4^+_2 member of the oblate deformed band.

The lifetimes were obtained using the gated $\gamma\gamma$ matrices and the singles spectra of rings 1 and 2 separately. The final values were obtained as an error-weighted average of all values. The results for the odd-spin yrast states are presented in Table III. In Table IV the results for the even-spin yrast states, obtained in the singles analysis, are compared to the results from the matrix analysis published in Ref. [8]. During the analysis of the singles spectra the assumption was made that the time behavior of unobserved feeding transitions is of the same order of magnitude than that of the observed feeding transition. The good agreement of the values obtained in singles and matrix analysis demonstrates the validity of these assumption

In the analysis utilizing the matrices the peaks were of low statistics, leading to large statistical errors. For the analysis using the singles spectra the high peak density resulted in several multiplets. Underlying peaks, even when they are weak, affect the ratio between both the shifted and unshifted components. If possible, the underlying peaks were integrated in the fit, thus the total intensity ratio $(I_{fs}, \gamma_1 + I_d, \gamma_1)/(I_{fs}, \gamma_i + I_d, \gamma_i)$ between the peaks from the transition of interest and the disturbing peaks were kept constant for all distances. The 472- and 748-keV transitions involved in the lifetime determination of the state at 1297.7-keV serve as very good examples for the previously mentioned difficulties. In the

TABLE III. Lifetimes of the odd-spin yrast states. Given are the level energy, the spin as assigned in the literature [22], the energy of the direct feeding $E_{\gamma,f}$ and depopulating $E_{\gamma,d}$ transition, and the lifetimes observed in the different approaches. The indices s stand for singles and m for matrix, 1 and 2 denote the respective rings of the JUROGAM array. For the calculation of the average values see text.

E_{Level} [keV]	J	$E_{\gamma,f}/E_{\gamma,d}$ [keV/keV]	τ_{s1} [ps]	τ_{s2} [ps]	$\overline{\tau_s}$ [ps]	τ_{m1} [ps]	τ_{m2} [ps]	$\overline{\tau}_m$ [ps]	$\overline{\tau}$ [ps]
1769.6	(5)	239/472[a]	<152	<152	<76	28(24)	35(14)	34(12)	34(12)
		239/1156	<152	<76	–	–	–	–	
2008.8	(7)	316/240	37.7(34)	35.3(33)	36.6(23)	37.4(45)	47(9)	39.3(40)	37.3(20)
		316/1062	38(8)	–	–	–	–		
2324.5	(9)	390/315	7.8(9)	10.2(10)	9.2(6)	8.7(14)	9.0(16)	8.8(10)	9.1(5)
		390/964	12(4)	10.2(17)		–	–	–	
2714.5	(11)	452/390	3.0(6)	3.1(4)	3.1(3)	3.2(9)	3.2(8)	3.2(6)	3.1(3)
3166.4	(13)	482[a]/452	1.5(5)	1.3(8)	1.4(5)	–	–	–	1.4(5)
3648.5	(15)	493[a]/482[a]	<3.8	<4.6	<3.8	–	–	–	<3.8

[a]Peak member of a multiplet.

singles spectra the peak of the 472-keV transition is situated in a group with the peaks of the 467- and 462-keV transitions. The energy difference between the fully-shifted, E_{fs}, and degraded, E_d, components [$\Delta(E_{\gamma,\text{fs}} - E_{\gamma,d})(470\ \text{keV}, 134^\circ) = 3.6$ keV; $\Delta(E_{\gamma,\text{fs}} - E_{\gamma,d})(470\ \text{keV}, 158^\circ) = 4.7$ keV] of the transitions with this particular γ-ray energy corresponds almost exactly to the difference between the individual γ transitions. In the analysis using the $\gamma\gamma$-coincidence matrices the peak contents after the background-subtracting gating process were too low. Thus the statistical errors ($E_\gamma = 749$ keV: $\Delta I \approx 50\%$) encountered in the peak fitting procedure prohibited any further lifetime analysis. In cases where no lifetimes could be determined, but at a given distance only the degraded component of the depopulating transition was observed, this distance was used to calculate an upper limit for the lifetime. The reaction kinematics resulted in 1 μm corresponding to 76 ns. Of course, the given values represent very conservative upper limits for the lifetimes, which in reality will probably be much shorter.

The lifetime of the $9^{(-)}$ state measured in this work for ^{182}Hg [$\tau(9^{(-)}) = 9.1(5)$ ps] and the lifetime of the 9^- state in ^{180}Hg [$\tau(9^-) = 10.2(12)$ ps] [8] are similar.

Resulting lifetimes for non-yrast states are presented in Table V. Due to the favored population of yrast states in fusion-evaporation reactions these states are poorly excited. Hence, the intensities of the depopulation transitions are low. Accordingly, only the singles analysis could be used; this led to uncertainties in some aspects of the analysis, as previously discussed. Consequently, as a result of these difficulties the lifetimes of the non-yrast states are rather uncertain.

IV. DISCUSSION

Assuming that the prolate-deformed intruder band and the odd-spin band form a well-deformed rotational system the Alaga rules [38] should be valid. The theoretical branching ratio R_{theo}, for the decays of a member of the negative parity band (J_i, K_i) to two members of the prolate deformed band ($J_{f,1}$, $K_{f,1}$; $J_{f,2}$, $K_{f,2}$) is given by

$$R_{\text{theo}} = \left| \frac{\sqrt{2J_{f,1}+1}\langle J_{f,1}K_{f,1}J_i(K_{f,1}-K_i)|J_iK_i\rangle}{\sqrt{2J_{f,2}+1}\langle J_{f,2}K_{f,2}J_i(K_{f,2}-K_i)|J_iK_i\rangle} \right|^2. \quad (1)$$

Comparison of the experimental branching ratio R_{exp}

$$R_{\text{exp}} = \frac{I(J_i \to J_{f,1})E^3_{\gamma,J_i\to J_{f,2}}}{I(J_i \to J_{f,2})E^3_{\gamma,J_i\to J_{f,1}}}, \quad (2)$$

to the possible theoretical values allows for the determination of the K-quantum number of the negative-parity band. The members of the odd-spin band with angular momentum $J^{(-)}$

TABLE IV. Lifetimes of the even-spin yrast states as obtained in the single analysis of this work. Given are the level energy, the spin J, the energies of the direct feeding $E_{\gamma,f}$ and depopulating $E_{\gamma,d}$ transitions, and the lifetimes observed. The indices 1 and 2 denote the respective rings of the JUROGAM array. Furthermore, the lifetimes of the matrix analysis published in Ref. [8] are repeated. For the calculation of the average values see text.

E_{Level} [keV]	J	$E_{\gamma,f}/E_{\gamma,d}$ [keV/keV]	$\tau_{s,1}$ [ps]	$\tau_{s,2}$ [ps]	$\overline{\tau_s}$ [ps]	$\overline{\tau}_m$ [ps]
351.8	2^+	262/352	36.4(38)	45.4(29)	42.1(23)	41(3)
613.2	4^+	333/262	37.1(8)	36.5(9)	37.1(11)	35.7(15)
		1156/261	<152	39.1(16)		
946.3	6^+	414/333	9.2(7)	9.1(9)	9.1(6)	8.2(5)
1360.3	8^+	488[a]/414	2.7(4)	3.0(4)	2.8(3)	2.9(3)
1847.7	10^+	553[a]/488[a]	–	1.44(32)	1.44(32)	1.2(3)

[a]Peak member of a multiplet.

TABLE V. Lifetimes of nonyrast states. Given are the level energy, the energies of the direct feeding $E_{\gamma,f}$ and depopulating $E_{\gamma,d}$ transitions, and the lifetimes observed in the singles mode. The indices 1 and 2 denote the respective rings of the JUROGAM array. The level placement is as shown in Fig. 3 of Ref. [22]. For the calculation of the average values see text.

E_{Level} [keV]	$E_{\gamma,f}/E_{\gamma,d}$ [keV/keV]	$\tau_{s,1}$ [ps]	$\tau_{s,2}$ [ps]	$\overline{\tau_s}$ [ps]
1297.7	472[a]/749	<152	<76	<76
1386	379/772	21.7(31)	16.5(36)	19.5(23)
1764	447[b]/379	5.9(11)	3.3(5)	3.8(5)
	447[b]/818	–	3.9(12)	
2212[c]	511[a]/379	–	3.0(23)	3.0(23)
2315	372[a]/302	22.1(47)	21.5(43)	21.8(32)

[a]Peak member of a multiplet.
[b]Peak contained in a second component.
[c]Value uncertain due to the involvement of the 511 keV γ rays.

in ^{182}Hg only show decays to the $(J-1)^+$ states of the prolate band, whereas the $J^\pi = 5^-$ state of the odd-spin band in ^{180}Hg decays to the $J^\pi = 4^+$ and 6^+ states of the prolate intruder band. The theoretical values are $R(\frac{5\to6}{5\to4}, K=0)_{\text{theo}} = 1.131$ and $R(\frac{5\to6}{5\to4}, K=1)_{\text{theo}} = 0.22$. The experimental value $R_{\text{exp}} = 1.07 \pm 0.14$ for ^{180}Hg agrees with the theoretical $R(K=0)$ value. Considering the striking similarities of the odd-spin bands in ^{180}Hg and ^{182}Hg we propose the assignment of $K=0$ to the odd-spin yrast band in ^{182}Hg. Possible admixtures of states belonging to the oblate deformed band into the wave functions of the spin-4 and spin-6 states of the prolate deformed band are considered to be negligible. However, applying the same method for the members of the odd-spin yrast band ($J \geqslant 7$) of ^{184}Hg [23] results in strongly deviating values. No systematic trend can be recognized, neither in the experimentally determined branching ratios R_{exp}, nor in comparison with the theoretical calculated values for any of the four possible K-quantum numbers.

The reduced transition probabilities, as given in Table VI and shown in Fig. 8, were calculated with the relative intensities and lifetimes obtained in this work. When in Fig. 3 of Ref. [22] a transition was assigned to be intraband exclusively the $B(E2)$ values are given. For the transitions connecting the suggested negative-parity and even-spin yrast bands an $E1$ multipolarity is probable. Consequently, for these transitions only the $B(E1)$ values are given. For interband transitions, for which the spin and parity of at least one of the states involved is not known, all the possible reduced transition probabilities $B(\pi, L)$ were calculated.

Within the rotational model the transition quadrupole moments Q_t, for intraband transitions can be calculated using

TABLE VI. Reduced transition probabilities $B(\pi, L)$ calculated using the relative intensities in Table I normalized for the respective state and the lifetimes given in Tables III, IV, and V, transition quadrupole moments $|Q_t|$ (for $K=0$) or dipole transition moments, $|D_t|$ and deformation parameters $|\beta_2^t|$. The horizontal lines group the respective levels of the two yrast bands and other observed levels. For a detailed discussion see text.

E_i [keV]	E_f [keV]	E_γ [keV]	J_i^π	J_f^π	$I_{\gamma,\text{rel}}$	τ [ps]	$B(E1)$ [10^{-3} W.u.]	$B(M1)$ [μ_N^2]	$B(E2)$ [W.u.]	$\lvert Q_t\rvert$ [e b]	$\lvert D_t\rvert$ [10^{-3} e b$^{1/2}$]	$\lvert\beta_2^t\rvert$
351.8	0	351.8	2^+	0^+	100	42.1(23)			55(3)	4.1(2)		0.15(1)
613.2	351.8	261.4	4^+	2^+	100	37.1(11)			253.1(75)	7.4(2)		0.26(1)
946.3	613.2	333.1	6^+	4^+	100	9.1(9)			331(33)	8.0(8)		0.29(3)
1360.3	946.3	413.7	8^+	6^+	100	2.8(3)			375(40)	8.4(9)		0.30(3)
1847.7	1360.3	487.4	10^+	8^+	100	1.44(32)			327(73)	7.7(11)		0.28(6)
1769.6	613.2	1156.4	$(5)^{(-)}$	4^+	15.9(55)	34(12)	0.001(1)				0.42(29)	
	1297.7	471.9	$(5)^{(-)}$		84.1(55)		0.07(3)	0.0121(51)	13.7(57)	–	3.7(15)	
2008.8	946.3	1062.5	$(7)^{(-)}$	6^+	16.8(75)	37.3(20)	0.001(1)				0.46(23)	
	1769.6	239.2	$(7)^{(-)}$	$(5)^{(-)}$	61.2(75)				230(41)	6.6(12)		0.24(4)
	1824.4	184.4	$(7)^{(-)}$		22.0(75)		0.26(10)	0.0224(88)	243(96)	–	7.0(28)	
2324.5	1360.3	964.2	$(9)^{(-)}$	8^+	26.9(47)	9.1(5)	0.010(2)				1.35(31)	
	2008.8	315.7	$(9)^{(-)}$	$(7)^{(-)}$	73.1(47)				313(37)	7.6(9)		0.27(3)
2714.5	1847.7	866.8	$(11)^{(-)}$	10^+	13.3(38)	3.1(3)	0.020(8)				1.90(73)	
	2324.5	389.9	$(11)^{(-)}$	$(9)^{(-)}$	86.7(38)				393(55)	8.4(12)		0.30(4)
3166.4	2714.5	482.1	$(13)^{(-)}$	$(11)^{(-)}$	100	1.4(5)			359(128)	8.0(28)		0.29(10)
1385.3	613.2	772.1		4^+	100	19.5(23)	0.034(4)	0.0062(7)	2.5(3)			
1764.4	946.3	818.1		6^+	46.7(67)	3.8(5)	0.068(19)	0.0124(34)	4.4(12)			
	1385.3	379.1			53.3(67)				226(58)			
2211.5	1360.3	851.2		8^+	33.3(75)	3.0(23)	0.055(54)	0.0100(99)	3.3(33)			
	1764.4	447.1			66.7(75)				160(141))			
2315.6	1360.3	955.2		8^+	weak	21.8(32)						
	1764.4	551.2			weak							
	2013.9	301.7			<100(11)				<221(56)			

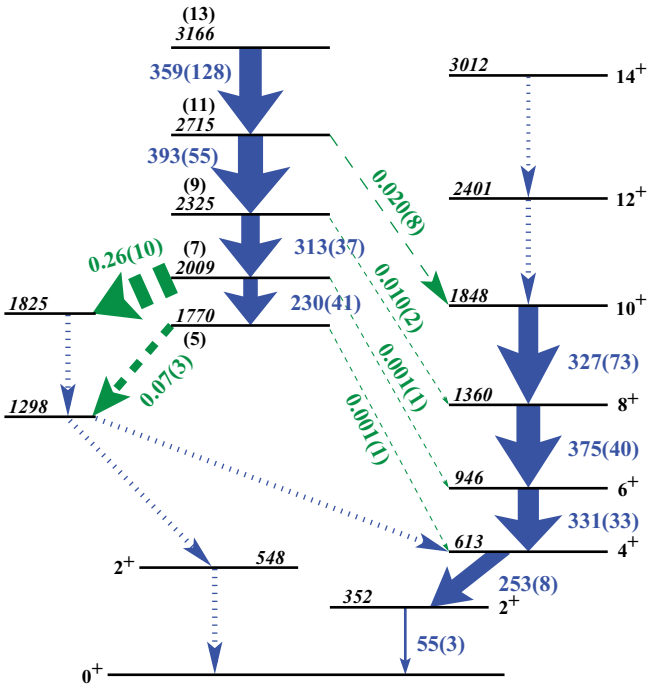

FIG. 8. (Color online) Partial level scheme of ^{182}Hg. The arrow widths are proportional to the observed $E2$ strength for intraband $E2$ transitions (straight line, blue) [W.u.] and assumed interband $E1$ transitions (dashed, green) [10^{-3} W.u.]. Arrows (short dashes) for which no strength is given correspond to observed transitions for which no transition strength could be obtained. For the transitions to the states at 1298 and 1825 keV the values for an assumed $E1$ multipolarity are plotted.

the formula [39]

$$B[E2, J \to (J-2)] = \frac{5}{16\pi}\langle J020|(J-2)0\rangle^2 Q_t^2. \quad (3)$$

For the calculation of the values presented in Table VI the K-quantum number was assumed to be $K = 0$. Variation of the Clebsch-Gordon coefficients for the possible K-quantum numbers changed the results by less than 10%. The trend as shown in Fig. 9 remains conserved for all four possible K-quantum numbers.

The transition quadrupole moments for the even-spin and the odd-spin yrast bands are shown in Fig. 9. The good agreement for both bands strongly supports the aligned nature of the $J = 3$ excitation to the even-spin band. Therefore, the underlying quadrupole deformation of the odd-spin states is given by the dynamical deformation of the mean field created by the respective state of the prolate-deformed, even-spin yrast band. Within small deviations the transitional quadrupole moments remain constant, indicating only minor changes in the structures for the quadrupole-deformation driving components of the wave functions with the increase of the rotational frequency. However, the slightly lower transition quadrupole moments for the low-spin member of the odd-spin band compared to the corresponding values of the even-spin band indicate a blocking. Quasiparticle excitations in the negative parity particle-hole channel occupy orbitals that are needed for the two-quasiparticle excitations creating the underlying prolate-deformed structure. The blocking decreases when, with increasing excitation energy, the number of two-quasiparticle components in the wave functions rises.

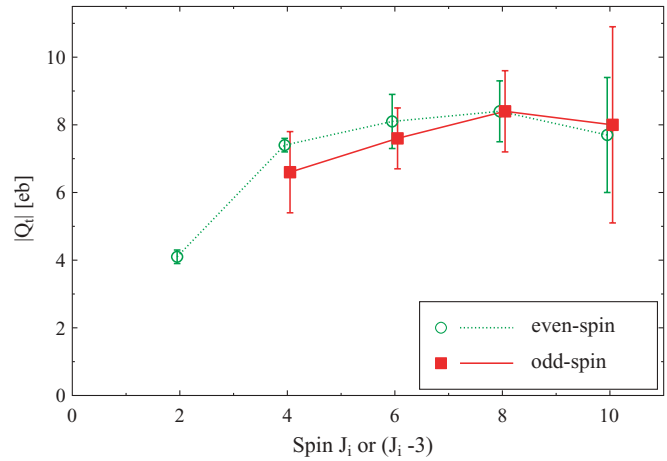

FIG. 9. (Color online) Transition quadrupole moments Q_t, of intraband transitions of the even-spin (green circles) and the odd-spin (red squares) yrast bands. The odd-spin states are shifted by three units of angular momentum. Furthermore, the values are slightly offset of their actual spin J_i value to maintain the clarity of the presentation.

Analogous to Eq. (3) for the transition quadrupole moment, a transition dipole moment D_t, for interband transitions connecting states of the odd-spin and even-spin yrast bands can be defined within the axially-symmetric rigid rotor model. To be consistent in the units we use for this work a modified version of Eq. (6a) from Ref. [40]

$$B[E1, J \to (J-1)] = \frac{3}{4\pi}\frac{J}{2J+1}D_t^2. \quad (4)$$

The calculated values (shown in Fig. 10) exhibit a trend of increasing transition dipole moments with increasing angular momentum. This can be understood by the means that due to the increasing rotational frequency the Coriolis force gradually weakens the pairing force. Therefore, the excitation energy of particle-hole excitations drops with increasing rotational

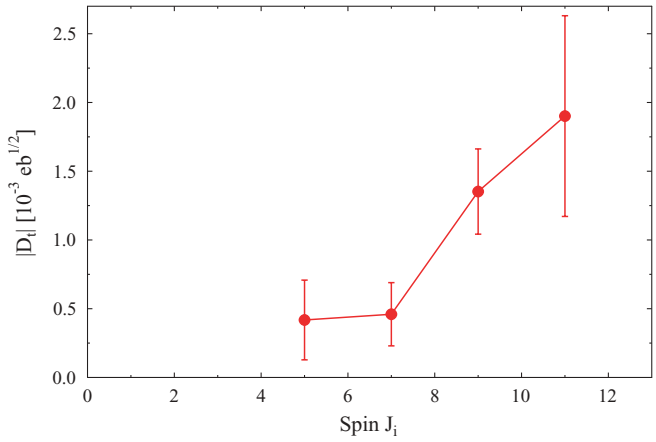

FIG. 10. (Color online) Transition dipole moments D_t, of interband transitions connecting states of the odd-spin and even-spin yrast bands.

frequency. In a geometric picture, the weakening of the pairing force and its spherical-shape restoring influence allows the nucleus a tendency toward an octupole shape with an increasing rotational frequency.

The absolute values of the $E1$ transition matrix elements connecting the odd-spin and even-spin yrast bands in ^{182}Hg are one to two orders of magnitude weaker than in nuclei with a pronounced octupole softness or even a tendency toward a stable octupole deformation (e.g., see Table 2 in Ref. [19]). The reason for the small overlap of the wave functions of the two bands can be found in their microscopic structures. The states of prolate deformed even-spin yrast band are dominated by proton two-quasiparticle excitations in the particle-particle as well as in the hole-hole channel, while the wave functions for the low-spin states of the odd-spin band can be expected to consist mainly of two-quasiparticle excitations in the particle-hole channel. To be included in these wave functions are the Nilsson orbitals originating from the neutron $\nu i_{13/2}$ subshell. Furthermore, in the prolate deformed field of the intruder configuration the low-Ω orbitals of the proton $h_{9/2}$, $f_{7/2}$, and $i_{13/2}$ subshells are shifted to lower energies, while the high-Ω orbits of the normal-parity subshells below the $Z = 82$ shell closure are shifted to higher energies. Calculations, using the formalism outlined in Ref. [41], predicted the two-quasiparticle energies for ^{178}Hg [17] and ^{178}Pt [42] for the first excited negative-parity two-quasineutron excitations below 2 MeV and the first excited negative-parity two-quasiproton excitations at approximately 2.5 MeV. This limited configuration space results in a low octupole collectivity.

To determine the absolute degree of octupole collectivity it is necessary to observe the $|J^-\rangle \rightarrow |(J-3)^+\rangle$ decay. However, in the spectrum at none of the possible energies ($E_{J^-} - E_{(J-3)^+}$) a peak was visible. Considering the hypothetical decay from the $J^\pi = 7^{(-)}$ state to the $J^\pi = 4_1^+$ state with $E_\gamma = 1384$ keV and one standard deviation of the background at this position in the spectra results in a relative intensity of 0.38% compared to the 351.7-keV transition. In combination with the other observed data of the $J^\pi = 7^{(-)}$ state the upper limit of the transition matrix element $|\langle 4_1^+|E3|7^{(-)}\rangle|$ is 730 e(fm)^3. Comparing this value to the value of 2450^{+70}_{-140} e(fm)^3 (Table 4 in Ref. [40]) as observed for the corresponding transition in ^{226}Ra, which is known to be situated in a region of the nuclear landscape with enhanced octupole correlations, it becomes obvious that the region of the light Hg nuclei has a rather low octupole collectivity.

The odd-spin band also shows decays to the two states at 1297.7 and 1824.4 keV connected via a 527.2 keV γ-ray transition. Assuming the 1297.7 and 1824.4-keV states form a band the interband $E2$ strength can be expected to be equal. However, for the 471.9-keV (13.7 ± 5.7 W.u.) and 183.9-keV (243 ± 96 W.u.) decays the corresponding $E2$ strengths will differ more than an order of magnitude and a dipole nature for these transitions is more likely. This results in comparably strong $E1$ or $M1$ transitions indicating a large overlap due to a similar microscopic structure of the wave functions of the odd-spin yrast band and these states.

V. SUMMARY AND CONCLUSION

Measured lifetimes for a sequence of low-spin members of the odd-spin yrast band in a light Hg nucleus allowed for the determination of transition quadrupole moments $|Q_t|$ and transition dipole moments $|D_t|$. The identical intraband transition quadrupole moments of odd-spin and even-spin yrast bands provide strong evidence that the negative parity excitation is aligned to the prolate deformed structure forming the even-spin yrast states.

The increase of the interband transition dipole moments $|D_t|$, of the transitions connecting states of odd-spin and even-spin yrast bands with spin of the respective states exhibits the expected behavior. However, the low interband $B(E1)$ values of the transitions connecting the two yrast bands confirm the low-degree of octupole collectivity in ^{182}Hg.

ACKNOWLEDGMENTS

This work was supported through EURONS (European Commission Contract No. RII3-CT-2004-506065), the Academy of Finland under the Finnish Centre of Excellence Programme 2006-2011 (Nuclear and Accelerator Based Physics Contract No. 213503), and the UK STFC. The UK/France (STFC/IN2P3) Loan Pool and GAMMAPOOL network are acknowledged for the EUROGAM detectors of JUROGAM. P.T.G. and C.S. acknowledge the support of the Academy of Finland, Contract Nos. 111965 and 209430, respectively.

[1] J. L. Wood, K. Heyde, W. Nazarewicz, M. Huyse, and P. van Duppen, Phys. Rep. **215**, 101 (1992).
[2] A. N. Andreyev *et al.*, Nature (London) **405**, 430 (2000).
[3] R. Julin, K. Helariutta, and M. Muikku, J. Phys. G **27**, R109 (2001).
[4] K. Heyde *et al.*, Nucl. Phys. **A466**, 189 (1987).
[5] S. Frauendorf and V. V. Pashkevich, Phys. Lett. **B55**, 365 (1975).
[6] R. Bengtsson and W. Nazarewicz, Z. Phys. A **334**, 269 (1989).
[7] W. Nazarewicz, Phys. Lett. **B305**, 195 (1993).
[8] T. Grahn *et al.*, Phys. Rev. C **80**, 014324 (2009).
[9] N. Rud *et al.*, Phys. Rev. Lett. **31**, 1421 (1973).
[10] D. Proetel *et al.*, Phys. Lett. **B48**, 102 (1974).
[11] W. C. Ma *et al.*, Phys. Lett. **B167**, 277 (1986).
[12] http://www.nndc.bnl.gov.
[13] P. Joshi *et al.*, Int. J. Mod. Phys. E **3**, 757 (1994).
[14] J. L. Wood, E. F. Zganjar, C. De Coster, and K. Heyde, Nucl. Phys. **A651**, 323 (1999).
[15] J. Wauters *et al.*, Phys. Rev. C **50**, 2768 (1994).
[16] G. D. Dracoulis, Phys. Rev. C **49**, 3324 (1994).
[17] F. G. Kondev *et al.*, Phys. Rev. C **62**, 044305 (2000).
[18] J. Pakarinen *et al.*, Phys. Rev. C **75**, 014302 (2007).
[19] P. A. Butler and W. Nazarewicz, Rev. Mod. Phys. **68**, 349 (1996).
[20] T. Kibédi and R. H. Spear, At. Data Nucl. Data Tables **80**, 35 (2002).
[21] F. G. Kondev *et al.*, Phys. Rev. C **61**, 011303(R) (1999).
[22] K. S. Bindra *et al.*, Phys. Rev. C **51**, 401 (1995).

[23] J. K. Deng *et al.*, Phys. Rev. C **52**, 595 (1995).
[24] M. G. Porquet *et al.*, J. Phys. G **18**, L29 (1992).
[25] W. C. Ma *et al.*, Phys. Rev. C **47**, R5 1993.
[26] M. Leino *et al.*, Nucl. Instrum. Methods B **99**, 653 (1995).
[27] R. D. Page *et al.*, Nucl. Instrum. Methods B **204**, 634 (2003).
[28] I. H. Lazarus *et al.*, IEEE Trans. Nucl. Sci. **48**, 567 (2001).
[29] P. Rahkila, Nucl. Instrum. Methods A **595**, 637 (2008).
[30] J. Wauters *et al.*, Z. Phys. A **345**, 21 (1993).
[31] A. Dewald, S. Harissopoulos, and P. von Brentano, Z. Phys. A **334**, 163 (1989).
[32] G. J. Lane, Nucl. Phys. **A589**, 129 (1995).
[33] D. T. Shi *et al.*, Phys. Rev. C **51**, 1720 (1995).
[34] W. F. Mueller *et al.*, Phys. Rev. C **59**, 2009 (1999).
[35] L. T. Song *et al.*, Phys. Rev. C **71**, 017302 (2005).
[36] P. Joshi *et al.*, Phys. Rev. C **66**, 044306 (2002).
[37] F. Somarel *et al.*, Eur. Phys. J. A **4**, 17 (1999).
[38] G. Alaga *et al.*, Dan. Mat. Fys. Medd. **29**, 1 (1955).
[39] T. Grahn *et al.*, Nucl. Phys. **A801**, 83 (2008).
[40] H. J. Wollersheim *et al.*, Nucl. Phys. **A556**, 261 (1993).
[41] F. G. Kondev *et al.*, Nucl. Phys. **A617**, 91 (1997).
[42] F. G. Kondev *et al.*, Phys. Rev. C **61**, 044323 (2000).